Climate Dynamics
https://doi.org/10.1007/s00382-018-4189-0

Evapotranspiration-dominated biogeophysical warming effect of urbanization in the Beijing-Tianjin-Hebei region, China

Guosong Zhao[1] · Jinwei Dong[1] · Yaoping Cui[2] · Jiyuan Liu[1] · Jun Zhai[3] · Tian He[4] · Yuyu Zhou[5] · Xiangming Xiao[6,7]

Received: 28 September 2017 / Accepted: 22 March 2018

Abstract
Given the considerable influences of urbanization on near-surface air temperature (T_a) and surface skin temperature (T_s) at local and regional scales, we investigated the biogeophysical effects of urbanization on T_a *and* T_s in the Beijing-Tianjin-Hebei (BTH) region of China, a typical rapidly urbanizing area, using the weather research and forecasting model (WRF). Two experiments were conducted using satellite-derived realistic areal fraction land cover data in 2010 and 1990 as well as localized parameters (e.g. albedo and leaf area index). Without considering anthropogenic heat, experimental differences indicated a regional biogeophysical warming of 0.15 °C (0.16 °C) in summer T_a (T_s), but a negligible warming in winter T_a (T_s). Sensitivity analyses also showed a stronger magnitude of local warming in summer than in winter. Along with an increase of 10% in the urban fraction, local T_a (T_s) increases of 0.185 °C (0.335 °C), 0.212 °C (0.464 °C), and 0.140 °C (0.220 °C) were found at annual, summer, and winter scales, respectively, according to a space-for-time substitution method. The sensitivity analyses will be beneficial to get a rough biogeophysical warming estimation of future urbanization projections. Furthermore, a decomposed temperature metric (DTM) method was applied for the attribution analyses of the change in T_s induced by urbanization. Our results showed that the decrease in evapotranspiration-induced latent heat played a dominate role in biogeophysical warming due to urbanization in BTH, indicating that increasing green space could alleviate warming effects, especially in summer.

Keywords Urbanization · Local effect · Surface energy balance · Numerical modeling

1 Introduction

By modifying the physical properties of the land surface, such as albedo, leaf area index (LAI), and roughness length, land use and land cover change (LULCC) alters exchanges of energy and water fluxes between land surfaces and the atmosphere, and with subsequent impacts on local and regional climate (Betts 2001; Feddema et al. 2005; Mahmood et al. 2014; Pielke et al. 2016; Pongratz et al. 2010). These above biogeophysical effects of LULCC are different from biogeochemical effects due to the emissions and deposition of carbon, nitrogen, and other chemically active species (de Noblet-Ducoudré et al. 2012; Feddema et al. 2005; Pielke et al. 2002, 2011; Pitman et al. 2009; Pongratz et al. 2010). Characterized by a large amount of natural

Electronic supplementary material The online version of this article (https://doi.org/10.1007/s00382-018-4189-0) contains supplementary material, which is available to authorized users.

✉ Jinwei Dong
dongjw@igsnrr.ac.cn

[1] Key Laboratory of Land Surface Pattern and Simulation, Institute of Geographic Sciences and Natural Resources Research, Chinese Academy of Sciences, Beijing 100101, China

[2] College of Environment and Planning, Henan University, Kaifeng 475004, China

[3] Satellite Environment Center, Ministry of Environmental Protection, Beijing 100094, China

[4] School of Water Conservancy and Environment, Zhengzhou University, Zhengzhou 450001, China

[5] Department of Geological and Atmospheric Sciences, Iowa State University, Ames, IA 50011, USA

[6] Department of Microbiology and Plant Biology, and Center for Spatial Analysis, University of Oklahoma, Norman, OK 73019, USA

[7] Ministry of Education Key Laboratory of Biodiversity Science and Ecological Engineering, Institute of Biodiversity Science, Fudan University, Shanghai 200433, China

Published online: 28 March 2018

or semi-natural vegetation and other land cover occupied by impervious surfaces, urbanization is a land use change form with the highest intensity of human influences. Despite minor urbanization impacts on national or global near-surface air temperature (T_a) (Solomon et al. 2007; Wang et al. 2015a), considerable influences on T_a or surface skin temperature (T_s, or land surface temperature), heat stress or precipitation are observed or modeled at local or regional scales, which cannot be ignored (Georgescu et al. 2013; Grimmond 2007; Niyogi et al. 2017; Oleson et al. 2015; Zhou et al. 2004). For example, the atmospheric/surface urban heat island (UHI) effect is a common phenomenon that results from urbanization (Li et al. 2017; Oke 1982; Stewart and Oke 2012; Voogt and Oke 2003).

Urbanization's climatic effects, particularly its influences on T_a/T_s, have been studied using many different approaches. Generally, the UMR (urban minus rural) (Hu et al. 2016; Ren and Ren 2011; Wang et al. 2017a) and OMR (observation minus reanalysis) (Kalnay and Cai 2003; Zhou et al. 2004) are two popular ways to quantify urbanization effects on T_a. However, the UMR is restricted by the spatial representation of meteorological observation sites, data inconsistency due to meteorological station relocation and equipment upgrading, and different selection standards for urban and rural sites (Cao et al. 2016b; Peterson 2003; Ren and Ren 2011); thus there is a potential uncertainty in final assessment results using the UMR method. OMR is also constrained by the influences of climate variability and various reanalysis datasets, which can result in inconsistent or contradictory results, or highly variable results among different reanalysis datasets (Wang et al. 2013a; Wang and Yan 2015). Although these two methods could be used to determine influences of urbanization on T_a, evaluation results are often site based or grid interpolated, and with biases and uncertainties. Remote sensing-based land surface temperature is often employed to quantify the spatial–temporal effects of urbanization on T_s (surface UHI). At present, more than ten indicators to quantify surface urban heat islands of cities have been explored (Clinton and Gong 2013; Li et al. 2017; Schwarz et al. 2011). However, quantified analyses about the mechanisms of urbanization impacts on T_a/T_s are absent in studies using these above methods based on observational data. Evaluations using the regional climate modeling (RCM) method at a finer spatial resolution provide an opportunity to detect biogeophysical effects of urbanization on T_a/T_s with greater spatial and temporal details, and also can provide a mechanism analysis from the perspective of surface energy balance, which is a meaningful and challenging work (Cao et al. 2016c; Georgescu et al. 2013; Sharma et al. 2017; Zhao et al. 2014).

In recent years, multiple modeling studies of climatic effects due to urbanization were carried out in cities, urban agglomerations and countries. However, there are still several primary shortcomings in these modeling studies. First, most studies evaluated the climatic effects of urbanization by virtual sensitivity experiments, which was completed by replacing urban areas with hypothesized land cover types (e.g., croplands, grasslands, or forests), instead of realistic land cover information (Wang et al. 2012, 2013b). Second, the dominant land cover type in a modeling grid was often adopted in the majority of simulations (Cao et al. 2016c; Zhao and Wu 2017), ignoring the mixture of different land cover types (Li et al. 2013). The above two shortcomings may lead to overestimated or underestimated urbanization-induced realistic climatic effects at local/regional levels. Third, the simulations often used an original look-up table of biogeophysical parameters based on averages at a global scale; thus localizing key biogeophysical parameters (e.g., albedo and LAI) is needed. Fourth, the sensitivity of local biogeophysical effects to urbanization has been rarely analyzed, specifically, how the local effects respond to an increase of 10% in urban fraction. Furthermore, local and nonlocal biogeophysical effects were seldom separated in the modeling studies (Kumar et al. 2013; Malyshev et al. 2015; Winckler et al. 2017a, b). Nonlocal effects refer to advection of local changes in air temperature and humidity caused by LULCC to nearby or remote regions (Winckler et al. 2017a, b). Finally, decomposition of contributions from the individual terms of the surface radiation/energy fluxes (or surface properties, such as albedo, Bowen ratio, aerodynamic resistance, surface resistance) to the change in T_s induced by LULCC was rarely conducted in previous studies.

Until now, three methods were proposed to separate contributions from the individual terms to the change in T_s due to LULCC. The first one is the decomposed temperature metric (DTM) method to analyze the change in T_s through changes in absorbed solar radiation, downward longwave radiation, sensible/latent heat flux, and ground heat flux (Juang et al. 2007; Luyssaert et al. 2014; Winckler et al. 2017a). The second one is the intrinsic biophysical mechanism (IBPM) method to separate the effects of albedo, aerodynamic resistance, Bowen ratio, surface storage and anthropogenic heat (Cao et al. 2016a; Lee et al. 2011; Zhao et al. 2014). The last one is the newly two-resistance mechanism (TRM) method to replacing the Bowen ratio in the IBPM method by the surface resistance (Rigden and Li 2017). Attribution of change in T_a/T_s is of great help to mitigate climate change. To our knowledge, although previous studies had considered two or three of the aforementioned shortcomings, none of these previous efforts took all the five aspects into account.

Motivated by previous studies and the aforementioned challenges, we aimed to examine the biogeophysical effects of urbanization with realistic and more precise land cover fraction information as well as localized parameters (e.g., albedo and LAI) embedded in the Weather Research and

Forecasting Model (WRF). The Beijing-Tianjin-Hebei (BTH) region of China, a highly urbanized hotspot, was taken as a case study area to evaluate the effects of urbanization on T_a and T_s. Moreover, we analyzed sensitivity of local biogeophysical effects to urbanization and further decomposed the individual contribution of changes in radiation/energy fluxes [e.g., net shortwave radiation flux (SW_{net}), latent heat flux (LE), and sensible heat flux (H)] to the change in T_s induced by urbanization.

2 Data and methods

2.1 Data

In WRF modeling, initial conditions and time-varying boundary conditions were taken from the ERA-Interim reanalysis dataset with a grid interval of $0.5° \times 0.5°$ and a time interval of 6 h (Dee et al. 2011). Albedo and LAI were retrieved from the Global LAnd Surface Satellite (GLASS) datasets for parameter localization (Liu et al. 2013; Xiao et al. 2016).

Land cover data of the BTH region were collected from the National Land Cover/Use Dataset of China (NLCD-China), which were produced by interpreting Landsat TM/ETM+ data. Based on field survey validation, classification accuracy for each land cover type in this dataset was over 90% (Liu et al. 2014, 2005). The original land cover/use data were aggregated as the areal fraction data with a grid interval of 4 km as same as the WRF modeling grids, then the fractional land cover data in 1990 and 2010 were incorporated in the WRF simulation grids for a better representation of mixture and fraction of different land cover types (see details in Sect. 2.2.1 and Fig. 1). In 1990–2010, urban expansion dominated the land use change across the whole the BTH region (Liu et al. 2014), other land use conversions, such as cropland reclamation, are quite limited. According to statistics, urban land fraction increased about 2% during 1990–2010 in the whole BTH region.

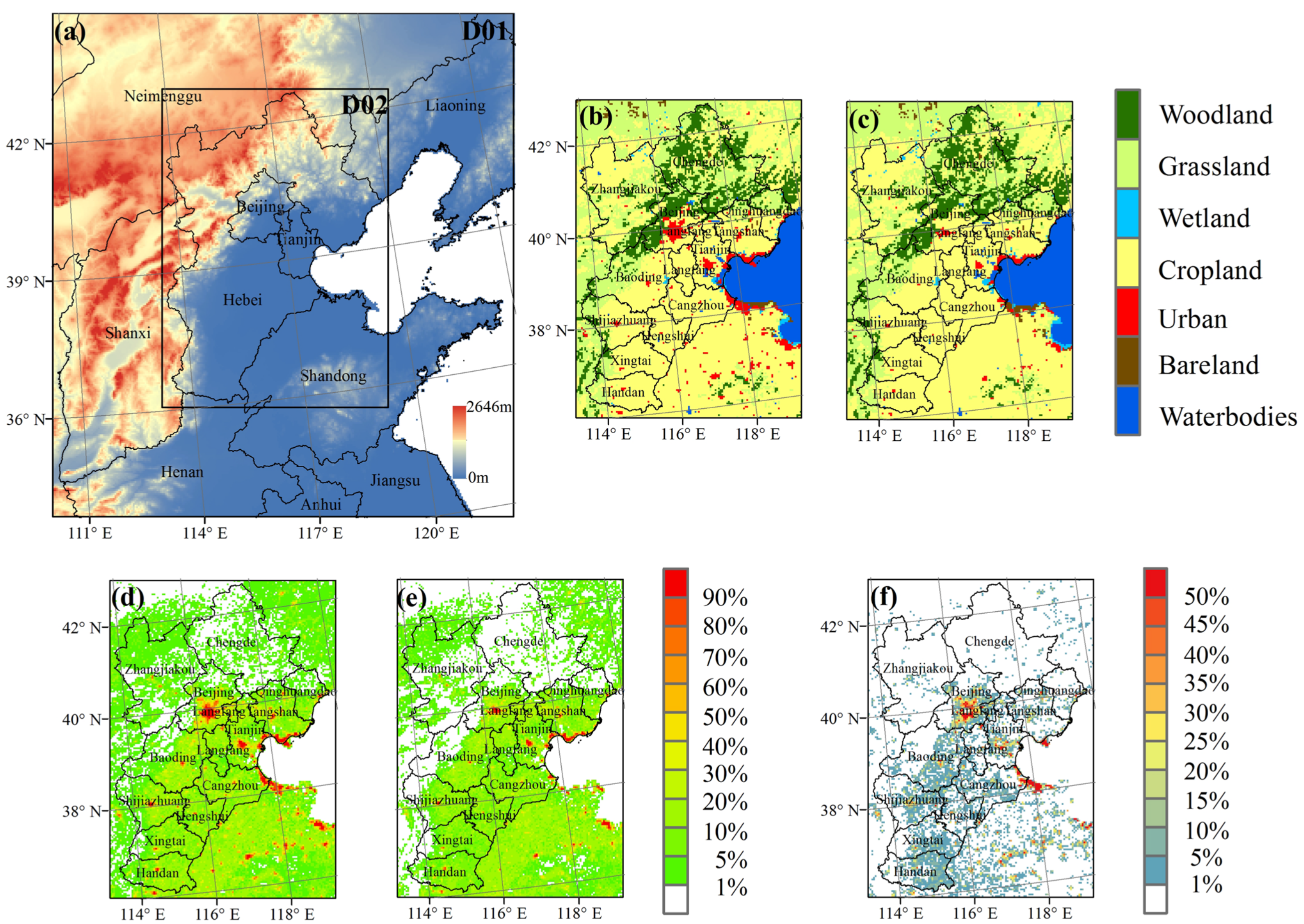

Fig. 1 Nested domains and land surface information in the WRF model configuration. **a** WRF model configuration for the two nested domains (D01 and D02) with the terrain height as background. The innermost domain (D02) covers the BTH region. **b** Land cover in 2010. **c** Land cover in 1990. **d** Urban fraction in 2010. **e** Urban fraction in 1990. **f** Change in the urban fraction during 1990–2010

Monthly T_a grid observation data in China at a grid interval of 0.5° from China Meteorological Data Service Center (CMDC), which were interpolated from about 2472 observational stations with a strict quality control, were used for validation of the WRF modeled results. Specifically, monthly averages of daily mean air temperature for 36 months (2009–2011) were used for the validation of modelling results in this study.

2.2 Methods

2.2.1 Design of experiments

Simulations were performed by using the WRF ARW version 3.6.1 (Skamarock and Klemp 2008). Two nested grids were used with grid interval of 20 km (domain 1) (56 × 61 grids) and 4 km (domain 2) (136 × 191 grids) (Fig. 1). Based on the land cover fraction data in 2010 and 1990 in the BTH region and surrounding areas, two experiments (Case2010 and Case1990) were designed for a 3-year simulation from December 1, 2008 to December 31, 2011, using the same initial and boundary conditions. The initial 31-day period (December 1–31 in 2008) was considered as a spin-up period to minimize the effects of the initial conditions. Effects of urbanization were quantified as the differences between the Case2010 and Case1990 experiments.

The parameterization schemes used in our simulation are listed in Table 1, and the WRF model setting details are as follows. In this study, the "mosaic/tiling" approach was adopted to represent sub-grid variability of different land cover types (i.e., urban land and other land types) within the modelling grids instead of the traditional "dominant land cover type" approach, thus for improving the simulations of surface radiation and turbulent fluxes (e.g., radiation, sensible heat, and latent heat fluxes) (Li et al. 2013). The first three land cover types with the highest area fractions, which accounted for more than 99% in all the grid cells, were considered in the WRF "mosaic/tiling" approach, while the other land cover types with limited fractions were ignored.

Table 1 Parameterization schemes in the WRF model configuration

Physical process	Parameterization scheme
Land surface process	Noah land surface model (Chen and Dudhia 2001; Li et al. 2013)
Longwave radiation scheme	RRTMG[a] (Iacono et al. 2008)
Shortwave radiation scheme	CAM[b] (Collins et al. 2004)
Microphysics scheme	WSM3[c] (Hong et al. 2004)
Cumulus scheme	Kain-Fritsch (Kain 2004)
Planetary boundary layer process	YSU[d] (Hong et al. 2006)

[a]RRTMG, a new version of rapid radiative transfer model

[b]CAM, the community atmosphere model shortwave radiation scheme

[c]WSM3, the WRF single-moment three-class microphysics scheme

[d]YSU, the Yonsei University planetary boundary layer scheme

The maximum and minimum values of albedo and LAI parameters are critical for accurately simulating the impacts of urban expansion on radiation and energy budgets, and then local/regional climate. Based on statistical analyses of quality-controlled albedo/LAI data from the GLASS product using the method of Zhao et al. (2017), the maximum and minimum values of albedo/LAI were extracted. Specifically, the maximum and minimum albedo of urban and built-up land (urban land for short, hereafter) in the original look-up table were updated to 0.153 and 0.138, while those of cropland were updated to 0.186 and 0.159, and grassland to 0.160 and 0.133, respectively, which were more accurate in our study area as a semi-humid zone. The maximum and minimum LAI values of urban land were updated to 0.497 and 0.104, which were apparently closer to the true value than original maximum and minimum values of 1, while the values for cropland were changed to 2.266 and 0.225, and grassland to 2.234 and 0.184, respectively.

2.2.2 Sensitivity of local biogeophysical effects to urbanization

Similar to the study of Winckler et al. (2017a), we assumed that the simulated total signal in grid cells experiencing urban expansion consisted of the sum of local and nonlocal effects. The nonlocal effects corresponded to that in grid cells without an additional urban expansion. As seen in Fig. 1f, a variety of changes in the urban fraction during 1990–2010 spread over the BTH region, indicating an opportunity to carry out a space-for-time substitution analysis. To separate local effects of urbanization from nonlocal effects, a simple space-for-time substitution method was proposed. A linear regression between the change in urban fraction (ΔF_u) and the change in T_a at 2 m (ΔT_a) (experimental differences between Case2010 and Case1990) at modeling grid cells (4 km × 4 km) in the BTH region was developed to explore the sensitivity of change in T_a to change in urban fraction, as shown in Eq. 1.

$$\Delta T_a = a1 \times \Delta F_U + b1. \tag{1}$$

In Eq. 1, the slope of $a1$ was treated as the local biogeophysical T_a effect when the urban fraction increased from 0 to 100%, and the constant $b1$ corresponded to the change in T_a without additional urban expansion, which was treated as a nonlocal T_a effect of urbanization. Sensitivity of local change in T_a to urbanization was defined by 10% of $a1$, which corresponded to local change in T_a due to an increase of urban fraction by 10%.

Similar analyses could also be performed for changes in radiation/energy fluxes and ΔF_u, as shown in Eq. 2, taking ΔLE as an example. The slope of $a2$ was treated as the local biogeophysical effect on LE when the urban fraction increased from 0 to 100%, $b2$ was treated as corresponding nonlocal effects on LE. Sensitivity of local change in LE to urbanization was defined by 10% of $a2$, which corresponded to local change in LE induced by an increase of urban fraction by 10%.

$$\Delta LE = a2 \times \Delta F_U + b2. \tag{2}$$

2.2.3 Decomposition of contributions of individual radiation/energy fluxes to change in T_s

An energy balance decomposition approach, the DTM method, was adopted to explore mechanisms controlling change in T_s induced by LULCC. This method is based on the surface energy balance, and a change in T_s due to LULCC can be split into contributions from the individual terms of the surface energy balance. The surface energy balance is:

$$SW_{net} + LW_{net} = R_n = H + LE + G, \tag{3}$$

$$SW_{net} = SW_{down} - SW_{up} = (1 - \alpha)SW_{down}, \tag{4}$$

$$LW_{net} = LW_{down} - LW_{up} = LW_{down} - \sigma T_s^{\ 4}, \tag{5}$$

where SW_{net} is the net shortwave radiation (or absorbed shortwave radiation), LW_{net} is the net longwave radiation, R_n is the net radiation, H is the sensible heat flux, LE is the latent heat flux, G is the ground heat flux, SW_{down} is the downward shortwave radiation, SW_{up} is the upward shortwave radiation, LW_{down} is the downward shortwave radiation, LW_{up} is the upward longwave radiation, α is the surface albedo, and σ is the Stefan–Boltzmann constant (5.67×10^{-8} W m^{-2} K^{-4}). Emissivity was set to 1 in the Eq. 5.

According to Juang et al. (2007), Luyssaert et al. (2014) and Winckler et al. (2017a), applying the first derivative of surface energy balance equation, change in T_s due to LULCC can be expressed as:

$$\Delta T_s = \lambda_0 \Delta SW_{net} + \lambda_0 \Delta SW_{down} - \lambda_0 \Delta H - \lambda_0 \Delta LE - \lambda_0 \Delta G, \tag{6}$$

$$\lambda_0 = \frac{1}{4\sigma T_s^3}, \tag{7}$$

where λ_0 is the local climate sensitivity according to Lee et al. (2011). In the right-hand side of Eq. 6, the five terms are isolated, representing individual contribution of change in absorbed shortwave radiation with albedo change (ΔSW_{net}), change in downward longwave radiation (ΔLW_{down}), change in sensible heat flux (ΔH), change in latent heat flux (ΔLE), and change in ground heat flux (ΔG).

3 Results

3.1 Model validation

To validate the performance of the WRF model, the simulation results of Case 2010 were compared with the grid observations from the CMDC from spatial and temporal aspects. As shown in Fig. 2, the WRF model reproduced the spatial variability of T_a fairly well compared with the grid observations, at annual, summer (June–July–August), and winter (December–January–February) scales. Specifically, the WRF model captured the lower T_a in northwestern part of the BTH region with high elevations, and higher T_a in plain regions. Generally, the T_a simulated using WRF was highly correlated with observations, with a spatial R^2 higher than 0.96 ($p < 0.001$) at annual, summer, and winter scales (Fig. 3a–c). However, the T_a simulated using WRF showed a positive bias compared with the observations, with a bias of 1.48 °C in annual scale, 1.75 °C in summer, and 1.37 °C in winter. Moreover, the simulated T_a captured the temporal variations (36 months) of observed T_a very well, and the correlations between them were very high, with a R^2 higher than 0.99 for the monthly averages ($p < 0.001$) (Fig. 3d). Overall, the WRF model can reproduce the spatial–temporal variations of T_a quite well, thus providing confidence in the model's capability to accurately capture the climatological characteristics in the BTH region.

3.2 Effects of urbanization on T_a and T_s

An increase of 0.10 °C in annual T_a due to urbanization was found in the BTH region from 1990 to 2010 based on the difference between the two experiments (Case2010–Case1990). Urbanization in the BTH region from 1990 to 2010 resulted in significant spatial and temporal variations in terms of change in T_a (Fig. 4a–c). Specifically, T_a increased over 1 °C in the areas experiencing an intensive urban expansion, such as surrounding areas of city centers of Beijing, Tianjin, and Shijiazhuang, while in woodland- or grassland-dominated areas, the change in T_a was small or negligible. Clear seasonal variations of urbanization effects were also found. Summer showed a larger temperature increase (0.15 °C) and a larger spatial domain (> 0.1 °C) than winter, indicating larger effects of urbanization in summer compared to those in winter. The change in T_s due to urbanization showed similar spatiotemporal patterns with that of T_a (Fig. 4d–f), and the regional average warming magnitude of T_s was slightly higher (about 0.01 °C) than T_a. However, in dramatic

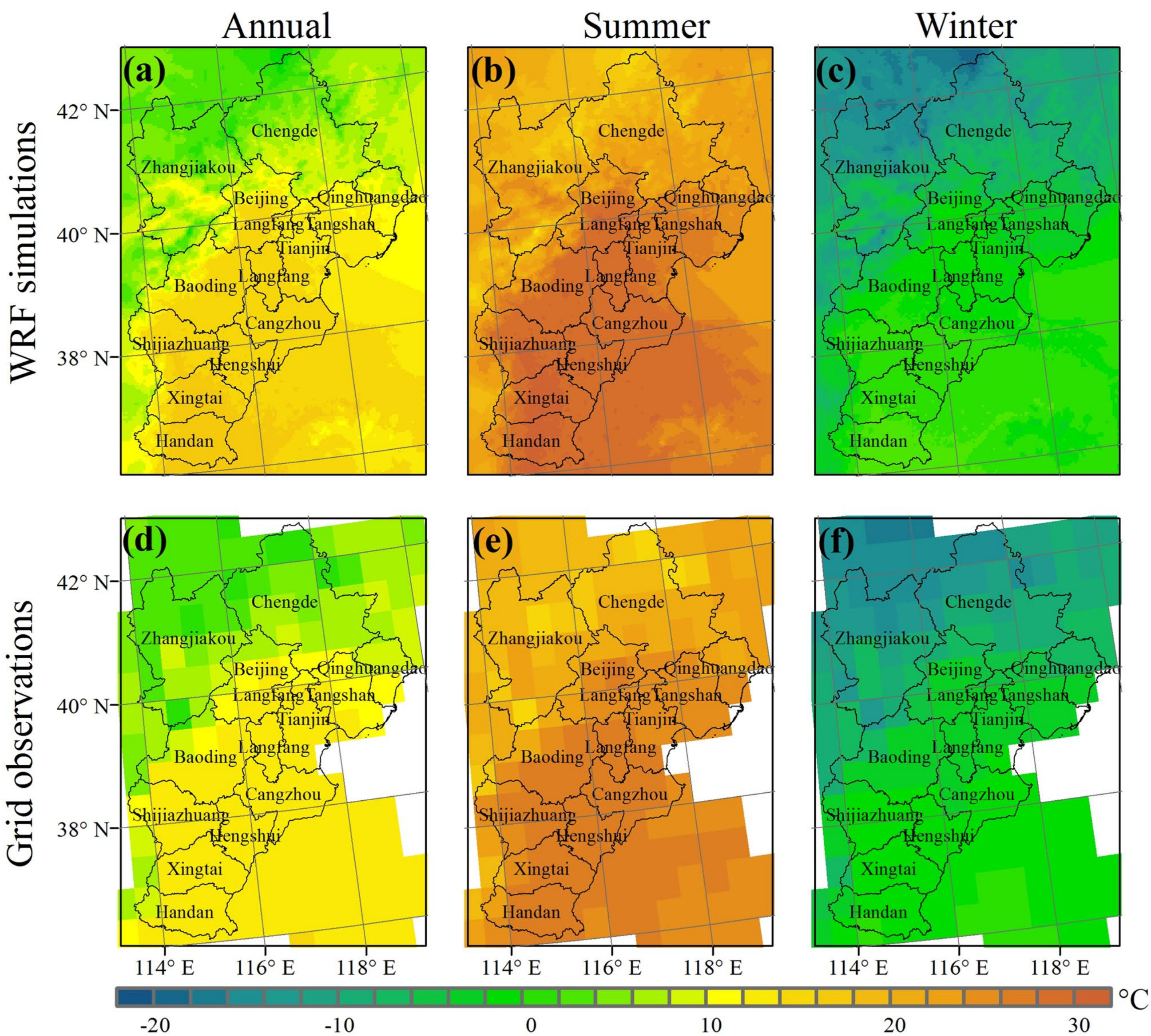

Fig. 2 Spatial comparison between the near-surface air temperature (T_a) from the WRF simulations (**a–c**) and the grid observations at the grid interval of 0.5° (**d–f**)

urbanizing areas, warming magnitude of T_s was much higher than T_a, as much as 2 °C, even higher than 3 °C in summer.

Strong and significant positive relationships between the changes in the urban fraction and the changes in $\Delta T_a/\Delta T_s$ were found (Fig. 5). The linear regression analyses showed that a change in the urban fraction from 0 to 100% induced a local warming in the annual T_a of 1.85 ± 0.008 °C (mean ± standard error). In summer, the warming magnitude was stronger as high as 2.12 ± 0.012 °C ($p < 0.001$), while in winter, the warming magnitude was much lower, with only a 1.40 ± 0.006 °C ($p < 0.001$) increase. In other words, the sensitivity of local T_a effect due to urbanization was 0.185, 0.212, and 0.140 °C corresponding with an increase of urban fraction by 10% at annual, summer, and winter scales, respectively. In terms of T_s, a change in the urban fraction from 0 to 100% induced a stronger local warming than T_a, with annual warming of 3.35 ± 0.011 °C, summer warming of 4.64 ± 0.021 °C, and winter warming of 2.20 ± 0.008 °C ($p < 0.001$). In other words, the sensitivity of local T_s effect due to urbanization was 0.335, 0.464 and 0.220 °C corresponding with an increase of urban fraction by 10% at annual, summer, and winter scales, respectively.

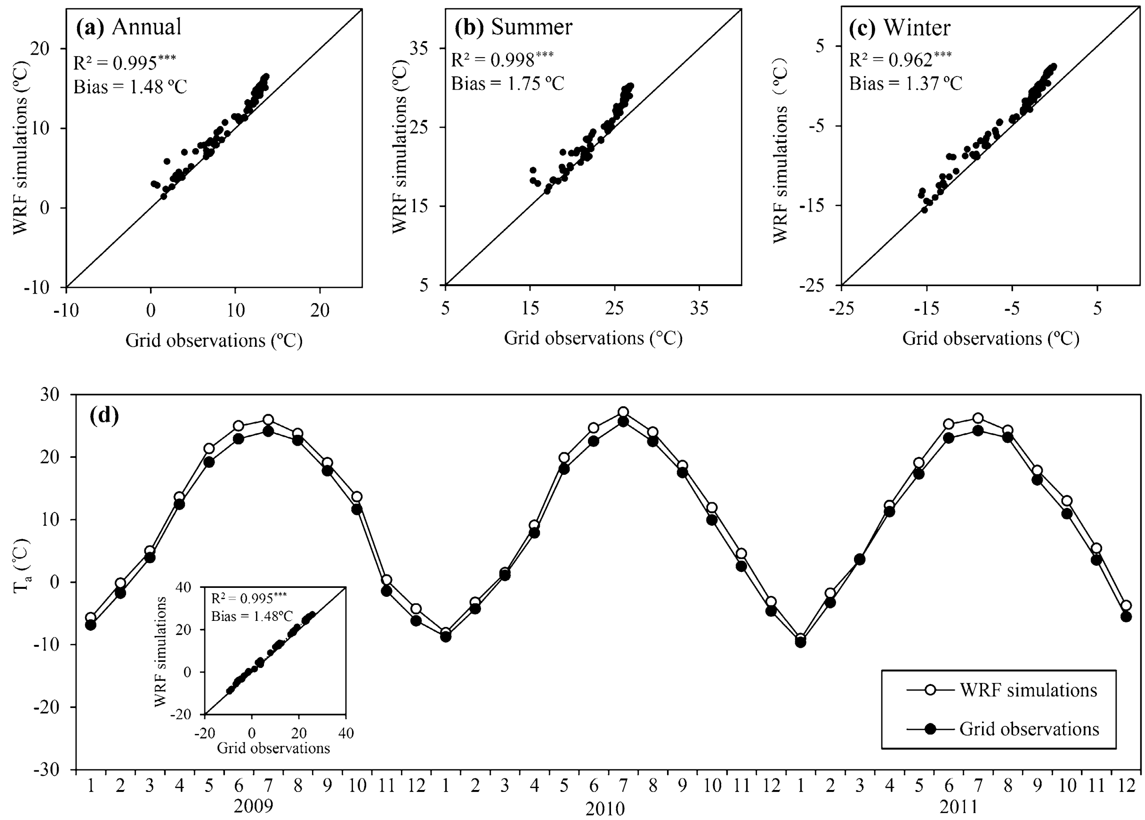

Fig. 3 Spatial and temporal comparisons between the near-surface air temperature (T_a) from the WRF simulations and the grid observations at the grid interval of 0.5°. **a–c** Spatial comparison at the grid interval of 0.5° at annual, summer, and winter scales, respectively. **d** Temporal comparison at the grid interval of 0.5° in the 36 months of 2009–2011. Significance level $^{***}p < 0.001$

3.3 Effects of urbanization on surface radiation/energy fluxes

Along with urbanization, albedo and LAI showed a decrease in the whole year, especially in the areas experiencing intensive urban expansion (Fig. 6). Because of the decrease in albedo (Fig. 6a–c) and the increase in T_s (Fig. 4d–f) after urbanization, remarkable changes in shortwave and longwave radiation flux occurred in the areas experiencing larger increases in the urban fraction, especially in terms of SW_{up} and LW_{up}. SW_{up} showed a decreasing trend due to the albedo decline when urban land encroached surrounding croplands during 1990–2010 (Fig. S1a), which resulted in more absorbed shortwave radiation on the surface (Fig. 7a). However, the LW_{up} showed an opposite trend with SW_{up} (Fig. S1b), with an increase trend due to higher T_s of urban lands than T_s of surrounding croplands (Fig. 4d–f), especially in summer, which resulted in a remarkable decrease in LW_{net}. Moreover, the LW_{down} also showed an increase trend due to higher T_a (Fig. 4a–c) induced by urbanization, especially in summer (Fig. 7b). Taking longwave and shortwave radiations together, R_n showed an annual decrease of 0.13 W m^{-2}, especially in the areas experiencing rapid urbanization (Fig. S1c). In summer, the decrease in R_n (− 0.43 W m^{-2}) was primarily caused by the increase of upward longwave radiation, which outweighed the increase of the absorbed shortwave radiation. However, in winter, R_n had a slight increase (0.07 W m^{-2}).

With paved and waterproofed surfaces owing high heat storage ability replacing moist soils and plants, urbanization in the BTH region has resulted in significant spatiotemporal variations for the sensible heat flux (H), latent heat flux (LE), and ground heat flux (Fig. 7). At an annual scale, LE decreased by 0.85 W m^{-2} across the BTH region, while H increased by 0.68 W m^{-2}, and G increased by only 0.05 W m^{-2}. LE showed a significant decrease throughout the year, especially in summer (− 1.93 W m^{-2}), while the change in LE was negligible in winter. H showed an opposite trend, especially in summer (1.40 W m^{-2}). Moreover, the areas with the most intensive urban expansion experienced the highest absolute magnitude of change in H/LE (> 40 W m^{-2}). G showed a similar increasing trend as H in summer, but with a much lower magnitude (0.14 W m^{-2}); however, G showed an opposite slight decreasing trend in winter.

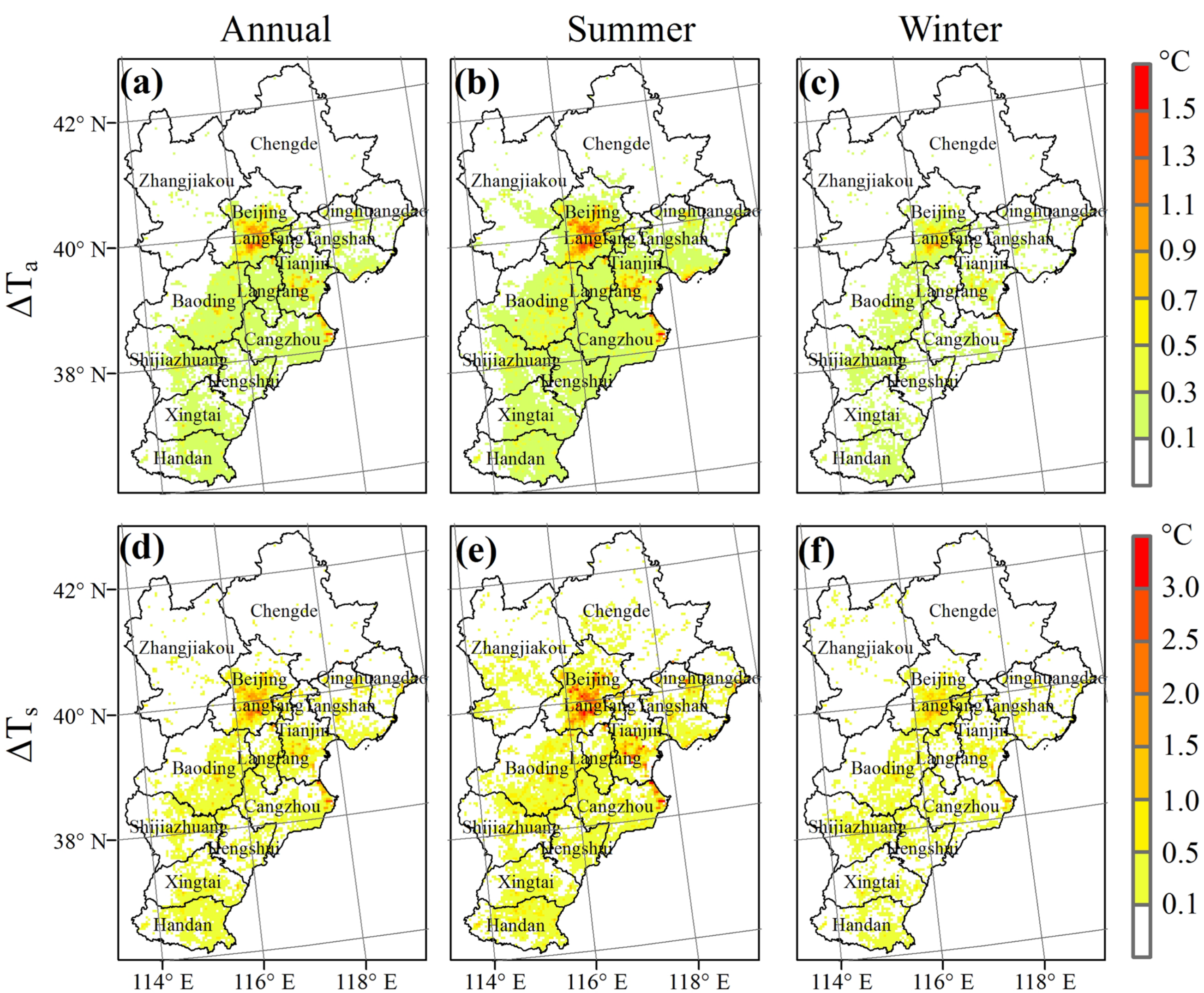

Fig. 4 Spatial pattern of urbanization effects on the near-surface air temperature (T_a) (**a**–**c**) and surface skin temperature (T_s) (**d**–**f**) at annual, summer, and winter scales

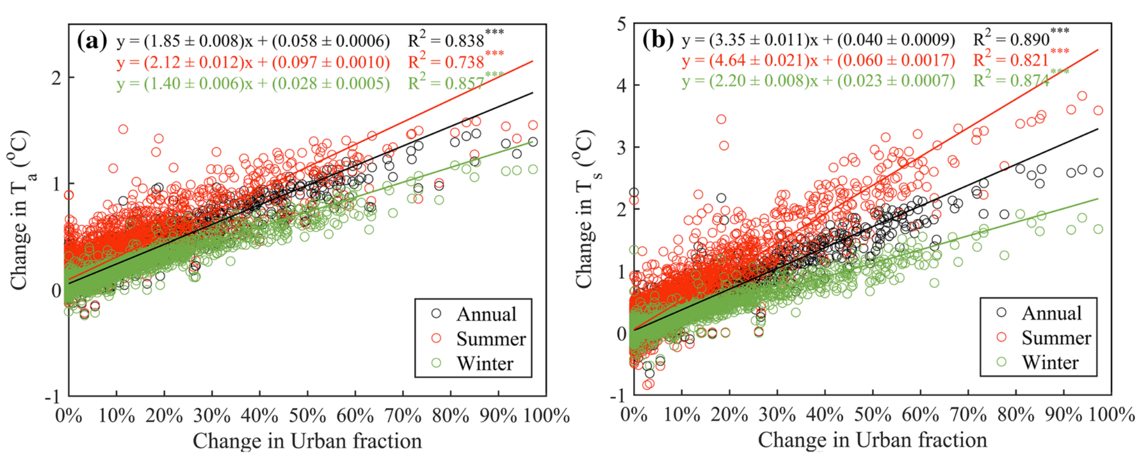

Fig. 5 Linear relationships between the changes in the urban fraction and the changes in T_a and T_s at annual, summer, and winter scales. Significance level $^{***}p < 0.001$

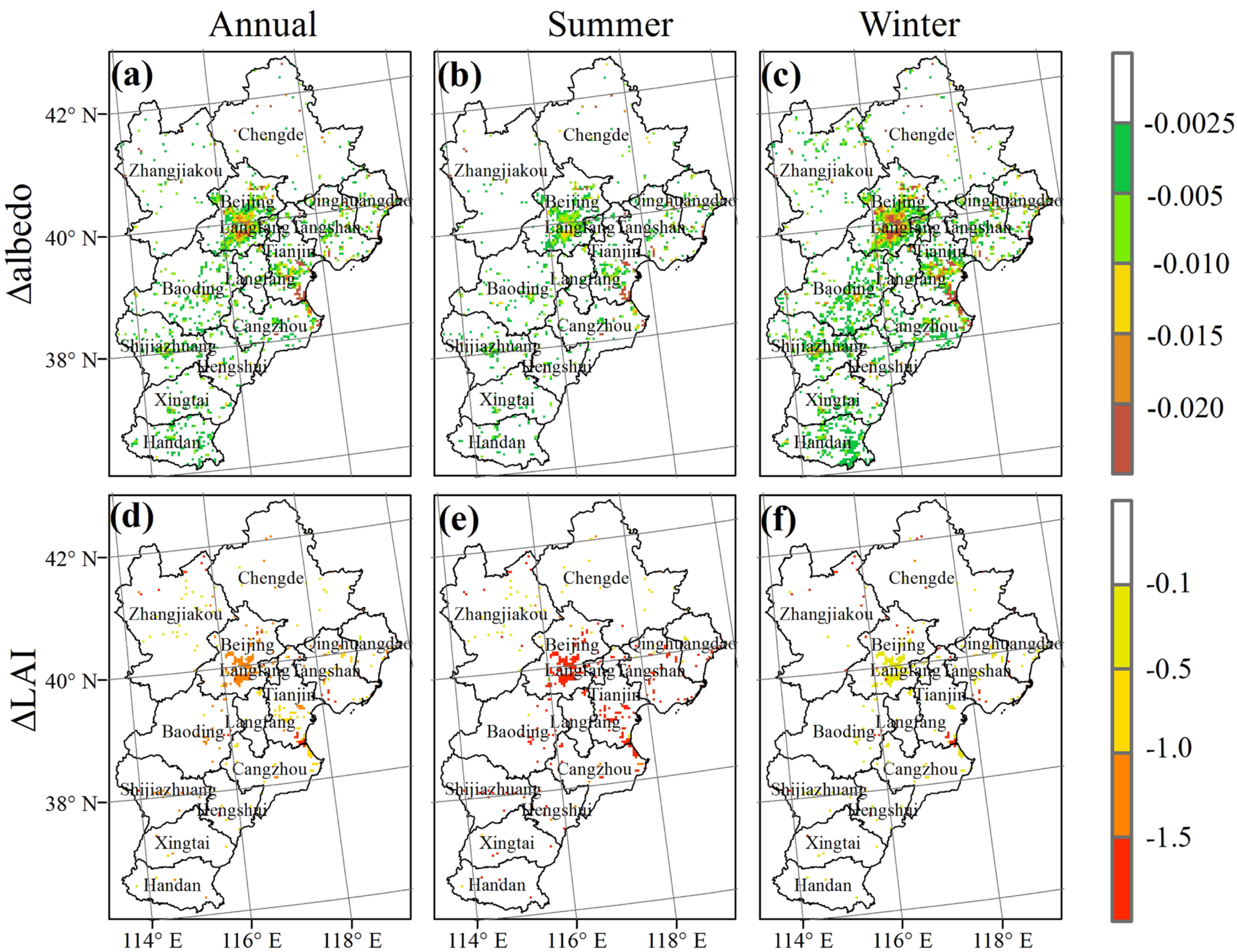

Fig. 6 Effects of urbanization on albedo (**a**–**c**) and leaf area index (LAI) (**d**–**f**) at annual, summer, and winter scales

Strong and significant relationships between the changes in urban fraction and changes in individual surface radiation/energy fluxes were also found (Fig. 8). At annual scale, *LE* showed a decreasing trend with an increase of urban fraction; specifically, a *LE* decrease of 4.78 W m^{-2} occurred along with a 10% increase in the urban fraction ($p < 0.001$), which indicated that urbanization significantly decreased *LE*. *H* showed an opposite, significant increasing trend with a decrease of 4.27 W m^{-2} along with a 10% increase in urban fraction ($p < 0.001$); that is, urbanization significantly increased *H*. Furthermore, SW_{net}, LW_{down}, *G*, and R_n increased or decreased slightly, with absolute changing rates less than 1 W m^{-2} ($p < 0.001$) along with a 10% change in urban fraction, indicating limited influences of urbanization on these fluxes (Fig. 8 and Fig. S2). Generally, ΔLE and ΔH in summer and winter showed a similar trend to that of the year, but with a larger magnitude of change in summer (slope = − 105.61 ± 0.354 and 87.35 ± 0.290 W m^{-2} for ΔLE and ΔH), and a smaller magnitude of change in winter, indicating a higher sensitivity in summer than winter. ΔR_n in summer showed a similar trend to that throughout the year, but a larger magnitude of change (slope = − 12.57 ± 0.183 W m^{-2}), while ΔR_n in winter showed an opposite trend (Fig. S2). The sensitivity of ΔSW_{net}, ΔLW_{down} or ΔG in summer or winter was also much lower than ΔLE *and* ΔH, less than 1 W m^{-2} change along with an increase of 10% in urban fraction. Among all these fluxes, the absolute change magnitude in *LE* was slightly greater than that in *H* and much greater than other fluxes, indicating *LE* was more sensitive to the increase in the urban fraction compared to *H* and other fluxes.

3.4 Contributions of five individual radiation/energy fluxes to the change in T_s

The WRF modelled results in grid cells with an urban fraction increase more than 60% were employed for analyzing component contribution of five individual radiation/energy

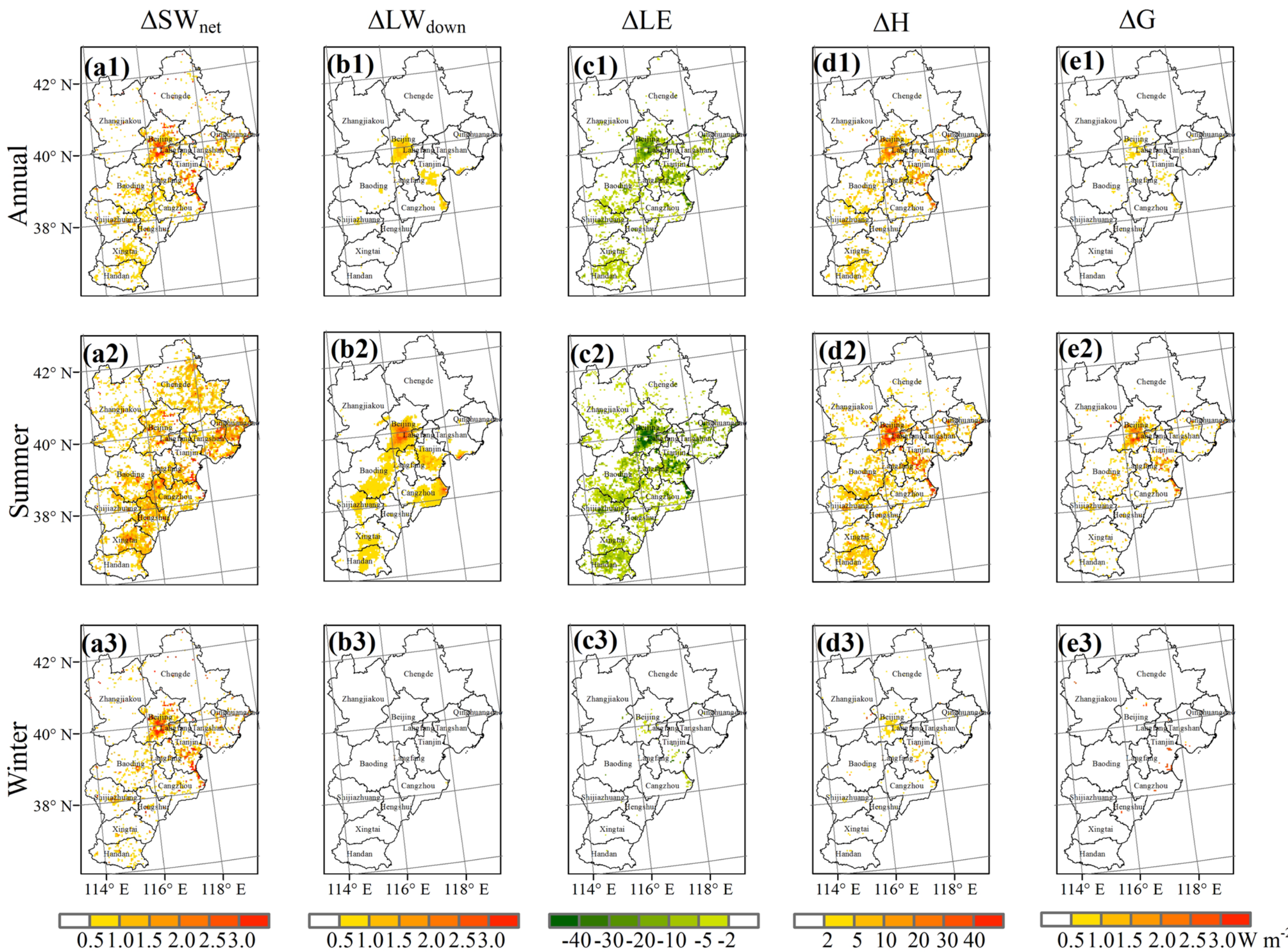

Fig. 7 Effects of urbanization on net shortwave radiation (SW_{net}) (**a1–a3**), downward longwave radiation (LW_{down}) (**b1–b3**), latent heat flux (LE) (**c1–c3**), sensible heat flux (H) (**d1–d3**), and ground heat flux (G) (**e1–e3**) at annual, summer, and winter scales

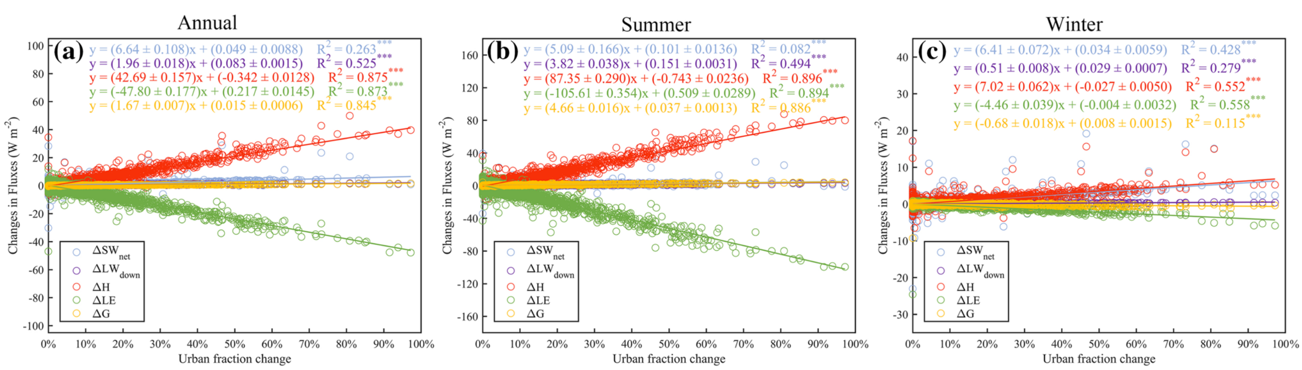

Fig. 8 Linear relationships between the changes in urban fraction and the changes in radiation/energy fluxes at annual, summer, and winter scales. Significance level $^{***}p < 0.001$

fluxes to the change in T_s. As shown in Fig. 9, the calculated ΔT_s (sum of contribution of five individual terms) by the DTM method agreed with WRF modeled ΔT_s very well. The calculated ΔT_s was about 0.7 °C lower than the WRF modelled ΔT_s either in annual scale or summer/winter scale. At annual scale, ΔLE contributed more than other four terms, indicating decrease in latent heat induced by urbanization dominated the biogeophysical warming effect, which

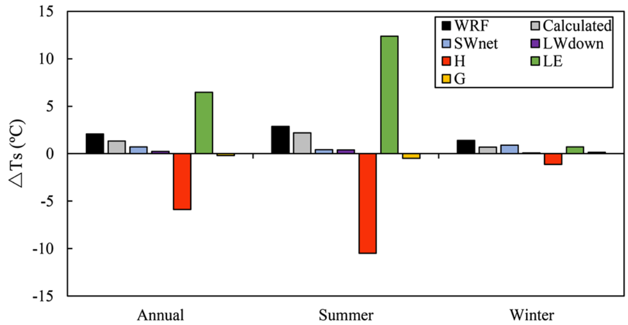

Fig. 9 Decomposition of contributions from five individual terms on ΔT_s induced by urbanization according to the DTM theory and WRF modelling results. Black bars denote ΔT_s by WRF modelling, grey bars denote ΔT_s calculated from the sum of the component contributions according to the DTM theory, light blue bars denote ΔT_s contributed by ΔSW_{net}, purple bars denote ΔT_s contributed by ΔLW_{down}, red bars denote ΔT_s contributed by ΔH, green bars denote ΔT_s contributed by ΔLE, and yellow bars denote ΔT_s contributed by ΔG

was more evident in the growing peak season of plants in summer. However, in winter, contribution of change in absorbed shortwave radiation along with albedo change was slightly higher than that of change in *LE*, indicating both the changes in absorbed shortwave radiation and *LE* dominated the warming effect in winter.

4 Discussion

4.1 Comparisons with existing studies in warming magnitude and seasonal pattern

In this study, we employed the bulk urban model instead of the urban canopy model (UCM), this setting missed the geometric features and the urban processes that UCM would describe more correctly, which may introduce modelling bias compared with the actual surface condition in the urban areas. However, our WRF modelling results showed a comparable accuracy with the studies of Cao et al. (2016c), Wang et al. (2012), and Wang et al. (2013b) using UCM, and they all showed modelling positive bias of about 1.5 °C, which may be related to the intrinsic limitations of WRF simulation.

The previous virtual sensitivity experiments of Wang et al. (2012, 2013b) were performed by replacing urban lands in the BTH region with adjacent land cover types; the warming magnitude in their studies was consistent with that in intensive urbanization areas (above 90%) in this study (Fig. 4). Warming magnitudes in both studies were higher than 1 °C, even as high as approximately 2 °C in summer. Moreover, a warming with such a magnitude was also found in realistic modeling studies by Cao et al. (2016c) and Zhao et al. (2017) in the BTH region. Stronger warming effects in summer than winter were also found in these studies, with an exception of Wang et al. (2013b), which considered anthropogenic heat. However, the larger spatial extent of warming in summer than winter that was demonstrated in this study agreed well with the aforementioned studies that involved seasonal variations.

The magnitude of local annual T_a increase (1.85 °C) with a change in urban fraction from 0 to 100% was also comparable with the observation-based studies (He et al. 2013; Yang et al. 2013). The study of He et al. (2013) established a relationship between change rates of the urban fraction and observational T_a during 1978–2008, and showed a 0.13 °C increase at annual scale with an increase of 10% in urban fraction. Yang et al. (2013) evaluated UHI intensity (UHII) over the Beijing Municipality by using 56 urban stations inside the 6th Ring Road and eight reference stations, whose result was quite similar to the result in this study. Specifically, Yang et al. (2013) found a daily average UHII of 1.65 °C inside the 4th Ring Road, which was a highly urbanized region covered with countless buildings and paved roads. Furthermore, the magnitude of local T_s increase was also comparable with remote sensing-based T_s studies within our study area (Cao et al. 2016a; Hu et al. 2015; Wang et al. 2017a; Zhao et al. 2017; Zhou et al. 2014). They all showed an annual T_s increase more than 2 °C at the annual scale, and a strong warming magnitude in summer than winter, even as much as 5–6 °C.

4.2 Comparisons with existing studies in warming mechanism

In this study, the absolute change in *LE* was slightly larger than that in *H* and much larger than other fluxes, indicating *LE* was the most sensitive flux with the increase in urban fraction, followed by *H*, while R_n and other fluxes were much less sensitive to urbanization, which is in line with previous studies based on observations (Guo et al. 2016; Wang et al. 2015b) and models (Cao et al. 2016c; Georgescu et al. 2009; Wang et al. 2012). Urbanization-induced increase of R_n in winter was found in the BTH region, which may be closely related to more absorbed incoming solar radiation from the large albedo decrease in winter (Fig. 6c), as well as less outgoing longwave radiation due to a lower daytime LST in urban areas compared to croplands, as reported in previous studies (Wang et al. 2017a; Zhao et al. 2017; Zhou et al. 2014).

According to the DTM method, we found that the decrease in evapotranspiration-induced *LE* dominated the biogeophysical warming due to urbanization in the BTH region, which has a temperate continental monsoon climate with a hot-wet summer and cold-dry winter. This finding was consistent with the perception that the evapotranspiration decrease due to vegetation loss is the dominant driver of daily surface temperature rise in the study of Wang et al. (2017b). Specifically, by employing flux observations in the urban and rural sites of Nanjing, Wang et al. (2017b) quantified the contribution of land surface factors to ΔT_s by considering the effects of surface albedo, roughness length, and evaporation using the IBPM method, and found that the evaporation decrease was the most important factor that modified the daily T_s change in the lower reaches of the Yangtze River valley.

4.3 Nonlocal effect analysis

The nonlocal effects of urbanization on T_a/T_s showed a consistent trend with the local effects of urbanization on T_a/T_s, both revealing a higher magnitude in summer than in winter (Fig. 5). This phenomenon was closely related to the strong air flow and horizontal heat advection in summer, indicating that the areas without additional urbanization were more easily influenced by remote areas with an intensive urbanization in summer than in winter. It is surprising that nonlocal effects of urbanization on *LE*/*H* at annual and summer scales were contrary to local effects, showing an increasing trend for *LE* and a decreasing trend for *H* (Fig. 8a, b). However, nonlocal effects of urbanization on R_n at annual and summer scales followed the same trend with those local effects (Fig. S2). Higher evapotranspiration rates in areas with abundant water would usually occur with higher T_a and T_s (Wang and Dickinson 2012; Wolf et al. 2016) indirectly influenced by remote urban sprawl areas, which may explain the increase in the nonlocal effects of *LE* influenced by local warming effects of remote urban sprawl areas. Nonlocal R_n decrease was similar to the local effects due to a higher T_s indirectly influenced by remote areas experiencing urban sprawl. As a result, nonlocal effects of urbanization on *H* showed a decreasing trend. Furthermore, nonlocal effects of urbanization on R_n/*LE*/*H* in winter were complex (Fig. 8c and Fig. S2c). Nonlocal R_n showed a slight decreasing trend in contrast with the local increasing effect, which was caused by more outward longwave radiation with higher T_s (Fig. 5b) and stable shortwave radiation with stable albedo. *LE* showed a slight decrease due to lower daytime T_s indirectly influenced by remote urban sprawl regions as discussed in Sect. 4.2, therefore *H* also showed a decreasing trend from the perspective of energy balance. Notably, nonlocal effects of the linear regression in this study were the average of the whole BTH region, yet nonlocal effects nearby regions experiencing intensive urban sprawl tended to be stronger than ones in regions with smaller urban sprawl (Figs. 4, 7).

4.4 Implications and future research

As indicated in previous studies (Chen and Frauenfeld 2015; Georgescu et al. 2013; Zhou et al. 2004), this study also showed that urbanization had strong and considerable local warming effects (> 2 °C in summer), requiring further attention in the context of increasing heat waves (Meehl and Tebaldi 2004; Sun et al. 2014; Wang et al. 2016). The sensitivity analysis of urbanization effects on surface skin or air temperature and radiation/energy fluxes will be of great help to get a rough estimation of biogeophysical effects in the future urbanization projections. In the BTH region, evapotranspiration-induced *LE* was the most sensitive flux to urbanization, and the decrease in evapotranspiration played the most important role in the biogeophysical warming effects from urbanization, indicating more vegetation (trees/grass) could reduce this strong warming effect.

The space-for-time substitution method in this study can not only identify the local biogeophysical effects but also evaluate the realistic effects, as opposed to the virtual control experiments in Winckler et al. (2017a). However, this method is limited to regions experiencing a large variety of land use change magnitude (0–100%) for carrying the space-for-time substitution analysis, and non-linear local/nonlocal effects due to urbanization is ignored, which suggests further research similar to the non-linear effects of deforestation denoted in Winckler et al. (2017b). Our experiments were performed for three continuous years using the WRF model by adopting the look-up table method, longer time integral simulation (20–30 years) with multi-mode sets (e.g., CCAM, CCSM, and ECHAM5) (Lejeune et al. 2017) would facilitate a more comprehensive understanding. Besides, incorporating realistic biophysical data (Cao et al. 2017; Vahmani and Ban-Weiss 2016) representing more accurate seasonal evolution of vegetation change instead of look-up table approach in the modelling process would facilitate analyses with lower uncertainty. In this study, biogeophysical effects induced by urbanization were investigated at a daily scale, different warming effects and mechanisms between daytime and nighttime (Cao et al. 2016a; McNider et al. 2012; Zhao et al. 2014) would improve our understanding on warming effects of urbanization, and is worth to be investigated in the near future. Moreover, the surface air moist enthalpy proposed by Pielke et al. (2004) could be an optimized metric for assessing surface global warming, which is worthy of more attention in future studies.

5 Conclusions

In this study, we performed experiments to investigate the biogeophysical effects of urbanization on T_a and T_s using the WRF model in an urbanization hotspot, the Beijing-Tianjin-Hebei Region, China. Land surface data were refined by incorporating the realistic fractional land cover data in 1990 and 2010 as well as localized parameters (i.e., LAI and albedo). A strong regional warming (0.15 °C) in summer was found, while the warming effect was negligible in winter. Sensitivity of local warming magnitude to urbanization was analyzed using a space-for-time substitution method. The results showed that with an increase of 10% in urban fraction, the magnitude of annual local T_a (T_s) warming was 0.185 °C (0.335 °C) with a decrease of 4.78 W m^{-2} in the corresponding latent heat flux (*LE)*; the magnitude of local T_a (T_s) warming in summer was much stronger with 0.212 °C (0.464 °C), and with a decrease of 10.56 W m^{-2} in *LE*; the warming magnitude in winter was less stronger. Compared with other surface energy balance terms, *LE* was the most sensitive flux to urbanization. Furthermore, the decrease in *LE* (or evapotranspiration) played the most important role in biogeophysical warming due to urbanization according to a DTM method, indicating that increasing green space could reduce this strong warming effect. The proposed space-for-time substitution method for identifying sensitivity of local biogeophysical effects of urbanization on T_a/T_s and R_n/*LE*/*H* is also applicable to other urbanized regions and other land use activities (e.g., deforestation/afforestation).

Acknowledgements This research is supported by the Strategic Priority Research Program (XDA19040301) and Key Research Program of Frontier Sciences (QYZDB-SSW-DQC005), the Chinese Academy of Sciences (CAS), the National Natural Science Foundation of China (41501484, 41671425, and 41701501), and the "Thousand Youth Talents Plan". We want to thank ECMWF for providing ERA-Interim reanalysis data (http://apps.ecmwf.int/datasets/), Global Land Cover Facility (GLCF) and Beijing Normal University for providing Global LAnd Surface Satellite (GLASS) albedo/LAI data (http://glcf.umd.edu/data/), and China Meteorological Data Service Center (CMDC) for providing grid air temperature observations (http://data.cma.cn/data/detail/dataCode/SURF_CLI_CHN_TEM_MON_GRID_0.5/). We also want to thank Xiaoming Hu from the University of Oklahoma and Jilin Yang from the Institute of Geographic Sciences and Natural Resources Research, CAS for their helps to improve the manuscript, as well as the three anonymous reviewers for their insightful comments.

References

Betts R (2001) Biogeophysical impacts of land use on present-day climate: near-surface temperature change and radiative forcing. Atmos Sci Lett 2:39–51. https://doi.org/10.1006/asle.2001.0023

Cao C, Lee X, Liu S, Schultz N, Xiao W, Zhang M, Zhao L (2016a) Urban heat islands in China enhanced by haze pollution. Nat Commun 7:12509. https://doi.org/10.1038/ncomms12509

Cao L, Zhu Y, Tang G, Yuan F, Yan Z (2016b) Climatic warming in China according to a homogenized data set from 2419 stations. Int J Climatol 36:4384–4392. https://doi.org/10.1002/joc.4639

Cao Q, Yu D, Georgescu M, Wu J (2016c) Impacts of urbanization on summer climate in China: an assessment with coupled land-atmospheric modeling. J Geophys Res Atmos 121:10505–10521. https://doi.org/10.1002/2016JD025210

Cao Q, Yu D, Georgescu M, Wu J (2017) Substantial impacts of landscape changes on summer climate with major regional differences: the case of China. Sci Total Environ 625:416. https://doi.org/10.1016/j.scitotenv.2017.12.290

Chen F, Dudhia J (2001) Coupling an advanced land surface-hydrology model with the Penn State–NCAR MM5 modeling system. Part I: model implementation and sensitivity. Mon Weather Rev 129:569–585

Chen L, Frauenfeld OW (2015) Impacts of urbanization on future climate in China. Clim Dyn 47:345–357. https://doi.org/10.1007/s00382-015-2840-6

Clinton N, Gong P (2013) MODIS detected surface urban heat islands and sinks: global locations and controls. Remote Sens Environ 134:294–304

Collins WD et al (2004) Description of the NCAR community atmosphere model (CAM 3.0). NCAR Technical Note NCAR/TN-464 + STR. https://doi.org/10.5065/D63N21CH

de Noblet-Ducoudré N et al (2012) Determining robust impacts of land-use-induced land cover changes on surface climate over North America and Eurasia: results from the first set of LUCID experiments. J Clim 25:3261–3281. https://doi.org/10.1175/JCLI-D-11-00338.1

Dee DP et al (2011) The ERA-Interim reanalysis: configuration and performance of the data assimilation system. Q J R Meteorolog Soc 137:553–597. https://doi.org/10.1002/qj.828

Feddema JJ, Oleson KW, Bonan GB, Mearns LO, Buja LE, Meehl GA, Washington WM (2005) The importance of land-cover change in simulating future climates. Science 310:1674–1678

Georgescu M, Miguez-Macho G, Steyaert LT, Weaver CP (2009) Climatic effects of 30 years of landscape change over the Greater Phoenix, Arizona, region: 1. Surface energy budget changes. J Geophys Res. https://doi.org/10.1029/2008jd010745

Georgescu M, Moustaoui M, Mahalov A, Dudhia J (2013) Summertime climate impacts of projected megapolitan expansion in Arizona. Nat Clim Change 3:37–41. https://doi.org/10.1038/nclimate1656

Grimmond S (2007) Urbanization and global environmental change: local effects of urban warming. Geogr J 173:83–88. https://doi.org/10.1111/j.1475-4959.2007.232_3.x

Guo W, Wang X, Sun J, Ding A, Zou J (2016) Comparison of land–atmosphere interaction at different surface types in the mid- to lower reaches of the Yangtze River valley. Atmos Chem Phys 16:9875–9890. https://doi.org/10.5194/acp-16-9875-2016

He Y, Jia G, Hu Y, Zhou Z (2013) Detecting urban warming signals in climate records. Adv Atmos Sci 30:1143–1153. https://doi.org/10.1007/s00376-012-2135-3

Hong S-Y, Dudhia J, Chen S-H (2004) A revised approach to ice microphysical processes for the bulk parameterization of clouds and precipitation. Mon Weather Rev 132:103–120

Hong S-Y, Noh Y, Dudhia J (2006) A new vertical diffusion package with an explicit treatment of entrainment processes. Mon Weather Rev 134:2318–2341

Hu Y, Jia G, Hou M, Zhang X, Zheng F, Liu Y (2015) The cumulative effects of urban expansion on land surface temperatures in metropolitan JingjinTang, China. J Geophys Res Atmos 120:9932–9943. https://doi.org/10.1002/2015jd023653

Hu X-M, Xue M, Klein PM, Illston BG, Chen S (2016) Analysis of urban effects in Oklahoma City using a dense surface observing network. J Appl Meteorol Clim 55:723–741. https://doi.org/10.1175/jamc-d-15-0206.1

Iacono MJ, Delamere JS, Mlawer EJ, Shephard MW, Clough SA, Collins WD (2008) Radiative forcing by long-lived greenhouse gases: calculations with the AER radiative transfer models. J Geophys Res Atmos. https://doi.org/10.1029/2008JD009944

Juang J-Y, Katul G, Siqueira M, Stoy P, Novick K (2007) Separating the effects of albedo from eco-physiological changes on surface temperature along a successional chronosequence in the southeastern United States. Geophys Res Lett. https://doi.org/10.1029/2007gl031296

Kain JS (2004) The Kain–Fritsch convective parameterization: an update. J Appl Meteorol 43:170–181

Kalnay E, Cai M (2003) Impact of urbanization and land-use change on climate. Nature 423:528. https://doi.org/10.1038/nature01675

Kumar S, Dirmeyer PA, Merwade V, DelSole T, Adams JM, Niyogi D (2013) Land use/cover change impacts in CMIP5 climate simulations: a new methodology and 21st century challenges. J Geophys Res Atmos 118:6337–6353. https://doi.org/10.1002/jgrd.50463

Lee X et al (2011) Observed increase in local cooling effect of deforestation at higher latitudes. Nature 479:384–387. https://doi.org/10.1038/nature10588

Lejeune Q, Seneviratne SI, Davin EL (2017) Historical land-cover change impacts on climate: comparative assessment of LUCID and CMIP5 multimodel experiments. J Clim 30:1439–1459. https://doi.org/10.1175/jcli-d-16-0213.1

Li D, Bou-Zeid E, Barlage M, Chen F, Smith JA (2013) Development and evaluation of a mosaic approach in the WRF-Noah framework. J Geophys Res Atmos 118:11918–11935. https://doi.org/10.1002/2013JD020657

Li X, Zhou Y, Asrar GR, Imhoff M, Li X (2017) The surface urban heat island response to urban expansion: a panel analysis for the conterminous United States. Sci Total Environ 605–606:426–435. https://doi.org/10.1016/j.scitotenv.2017.06.229

Liu J et al (2005) Spatial and temporal patterns of China's cropland during 1990–2000: an analysis based on Landsat TM data. Remote Sens Environ 98:442–456. https://doi.org/10.1016/j.rse.2005.08.012

Liu Q, Wang L, Qu Y, Liu N, Liu S, Tang H, Liang S (2013) Preliminary evaluation of the long-term GLASS albedo product. Int J Digital Earth 6:69–95. https://doi.org/10.1080/17538947.2013.804601

Liu J et al (2014) Spatiotemporal characteristics, patterns, and causes of land-use changes in China since the late 1980s. J Geog Sci 24:195–210. https://doi.org/10.1007/s11442-014-1082-6

Luyssaert S et al (2014) Land management and land-cover change have impacts of similar magnitude on surface temperature. Nat Clim Change 4:389–393. https://doi.org/10.1038/nclimate2196

Mahmood R et al (2014) Land cover changes and their biogeophysical effects on climate. Int J Climatol 34:929–953. https://doi.org/10.1002/joc.3736

Malyshev S, Shevliakova E, Stouffer RJ, Pacala SW (2015) Contrasting local versus regional effects of land-use-change-induced heterogeneity on historical climate: analysis with the GFDL earth system model. J Clim 28:5448–5469. https://doi.org/10.1175/JCLI-D-14-00586.1

McNider RT et al (2012) Response and sensitivity of the nocturnal boundary layer over land to added longwave radiative forcing. J Geophys Res Atmos. https://doi.org/10.1029/2012jd017578

Meehl GA, Tebaldi C (2004) More intense, more frequent, and longer lasting heat waves in the 21st century. Science 305:994–997. https://doi.org/10.1126/science.1098704

Niyogi D, Lei M, Kishtawal C, Schmid P, Shepherd M (2017) Urbanization impacts on the summer heavy rainfall climatology over the eastern United States. Earth Interact 21:1–17. https://doi.org/10.1175/ei-d-15-0045.1

Oke TR (1982) The energetic basis of the urban heat island. Q J R Meteorolog Soc 108:1–24. https://doi.org/10.1002/qj.49710845502

Oleson K et al (2015) Interactions between urbanization, heat stress, and climate change. Clim Change 129:525–541

Peterson TC (2003) Assessment of urban versus rural in situ surface temperatures in the contiguous United States: no difference found. J Clim 16:2941–2959

Pielke RA et al (2002) The influence of land-use change and landscape dynamics on the climate system: relevance to climate-change policy beyond the radiative effect of greenhouse gases. Philos Trans R Soc A 360:1705–1719. https://doi.org/10.1098/rsta.2002.1027

Pielke RA, Davey C, Morgan J (2004) Assessing "global warming" with surface heat content. Eos Trans Am Geophys Union 85:210–211

Pielke RA et al (2011) Land use/land cover changes and climate: modeling analysis and observational evidence. Wiley Interdiscip Rev Clim Change 2:828–850. https://doi.org/10.1002/wcc.144

Pielke RA, Mahmood R, McAlpine C (2016) Land's complex role in climate change. Phys Today 69:40–46. https://doi.org/10.1063/pt.3.3364

Pitman AJ et al. (2009) Uncertainties in climate responses to past land cover change: first results from the LUCID intercomparison study. Geophys Res Lett. https://doi.org/10.1029/2009gl039076

Pongratz J, Reick C, Raddatz T, Claussen M (2010) Biogeophysical versus biogeochemical climate response to historical anthropogenic land cover change. Geophys Res Lett. https://doi.org/10.1029/2010GL043010

Ren Y, Ren G (2011) A remote-sensing method of selecting reference stations for evaluating urbanization effect on surface air temperature trends. J Clim 24:3179–3189. https://doi.org/10.1175/2010JCLI3658.1

Rigden AJ, Li D (2017) Attribution of surface temperature anomalies induced by land use and land cover changes. Geophys Res Lett 44:6814–6822. https://doi.org/10.1002/2017GL073811

Schwarz N, Lautenbach S, Seppelt R (2011) Exploring indicators for quantifying surface urban heat islands of European cities with MODIS land surface temperatures. Remote Sens Environ 115:3175–3186. https://doi.org/10.1016/j.rse.2011.07.003

Sharma A, Fernando HJS, Hamlet AF, Hellmann JJ, Barlage M, Chen F (2017) Urban meteorological modeling using WRF: a sensitivity study. Int J Climatol 37:1885–1900. https://doi.org/10.1002/joc.4819

Skamarock WC, Klemp JB (2008) A time-split nonhydrostatic atmospheric model for weather research and forecasting applications. J Comput Phys 227:3465–3485. https://doi.org/10.1016/j.jcp.2007.01.037

Solomon S et al (eds) (2007) Climate change 2007-the physical science basis: working group I contribution to the fourth assessment report of the IPCC. Cambridge University Press, Cambridge

Stewart ID, Oke TR (2012) Local climate zones for urban temperature studies. Bull Am Meteorol Soc 93:1879–1900. https://doi.org/10.1175/bams-d-11-00019.1

Sun Y et al (2014) Rapid increase in the risk of extreme summer heat in Eastern China. Nat Clim Change 4:1082–1085. https://doi.org/10.1038/nclimate2410

Vahmani P, Ban-Weiss GA (2016) Impact of remotely sensed albedo and vegetation fraction on simulation of urban climate in WRF-urban canopy model: a case study of the urban heat island in Los Angeles. J Geophys Res Atmos 121:624–624. https://doi.org/10.1002/2015JD023718

Voogt JA, Oke TR (2003) Thermal remote sensing of urban climates. Remote Sens Environ 86:370–384. https://doi.org/10.1016/S0034-4257(03)00079-8

Wang K, Dickinson RE (2012) A review of global terrestrial evapotranspiration: observation, modeling, climatology, and climatic variability. Rev Geophys. https://doi.org/10.1029/2011RG000373

Wang M, Yan X (2015) A comparison of two methods on the climatic effects of urbanization in the Beijing-Tianjin-Hebei metropolitan area. Adv Meteorol 2015:1–12. https://doi.org/10.1155/2015/352360

Wang J, Feng J, Yan Z, Hu Y, Jia G (2012) Nested high-resolution modeling of the impact of urbanization on regional climate in three vast urban agglomerations in China. J Geophys Res Atmos 117:D21103. https://doi.org/10.1029/2012jd018226

Wang J, Yan Z, Jones PD, Xia J (2013a) On "observation minus reanalysis" method: a view from multidecadal variability. J Geophys Res Atmos 118:7450–7458. https://doi.org/10.1002/jgrd.50574

Wang M, Zhang X, Yan X (2013b) Modeling the climatic effects of urbanization in the Beijing–Tianjin–Hebei metropolitan area. Theor Appl Climatol 113:377–385. https://doi.org/10.1007/s00704-012-0790-z

Wang F, Ge Q, Wang S, Li Q, Jones PD (2015a) A new estimation of urbanization's contribution to the warming trend in China. J Clim 28:8923–8938. https://doi.org/10.1175/JCLI-D-14-00427.1

Wang L, Gao Z, Miao S, Guo X, Sun T, Liu M, Li D (2015b) Contrasting characteristics of the surface energy balance between the urban and rural areas of Beijing. Adv Atmos Sci 32:505. https://doi.org/10.1007/s00376-014-3222-4

Wang J, Yan Z, Quan X-W, Feng J (2016) Urban warming in the 2013 summer heat wave in eastern China. Clim Dyn 48:3015–3033. https://doi.org/10.1007/s00382-016-3248-7

Wang K, Jiang S, Wang J, Zhou C, Wang X, Lee X (2017a) Comparing the diurnal and seasonal variabilities of atmospheric and surface urban heat islands based on the Beijing urban meteorological network. J Geophys Res Atmos 122:2131–2154. https://doi.org/10.1002/2016JD025304

Wang X, Guo W, Qiu B, Liu Y, Sun J, Ding A (2017b) Quantifying the contribution of land use change to surface temperature in the lower reaches of the Yangtze River. Atmos Chem Phys 17:4989–4996. https://doi.org/10.5194/acp-17-4989-2017

Winckler J, Reick CH, Pongratz J (2017a) Robust identification of local biogeophysical effects of land-cover change in a global climate model. J Clim 30:1159–1176. https://doi.org/10.1175/jcli-d-16-0067.1

Winckler J, Reick CH, Pongratz J (2017b) Why does the locally induced temperature response to land cover change differ across scenarios? Geophys Res Lett 44:3833–3840. https://doi.org/10.1002/2017gl072519

Wolf S et al (2016) Warm spring reduced carbon cycle impact of the 2012 US summer drought. PNAS 113:5880–5885. https://doi.org/10.1073/pnas.1519620113

Xiao Z, Liang S, Wang J, Xiang Y, Zhao X, Song J (2016) Long-time-series global land surface satellite leaf area index product derived from MODIS and AVHRR surface reflectance. IEEE Trans Geosci Remote Sens 54:5301–5318. https://doi.org/10.1109/TGRS.2016.2560522

Yang P, Ren G, Liu W (2013) Spatial and temporal characteristics of Beijing urban heat island intensity. J Appl Meteorol Clim 52:1803–1816. https://doi.org/10.1175/jamc-d-12-0125.1

Zhao D, Wu J (2017) The influence of urban surface expansion in china on regional climate. J Clim 30:1061–1080. https://doi.org/10.1175/jcli-d-15-0604.1

Zhao L, Lee X, Smith RB, Oleson K (2014) Strong contributions of local background climate to urban heat islands. Nature 511:216–219. https://doi.org/10.1038/nature13462

Zhao G, Dong J, Liu J, Zhai J, Cui Y, He T, Xiao X (2017) Different patterns in daytime and nighttime thermal effects of urbanization in Beijing-Tianjin-Hebei urban agglomeration. Remote Sens 9:121. https://doi.org/10.3390/rs9020121

Zhou L et al (2004) Evidence for a significant urbanization effect on climate in China. PNAS 101:9540–9544. https://doi.org/10.1073/pnas.0400357101

Zhou D, Zhao S, Liu S, Zhang L, Zhu C (2014) Surface urban heat island in China's 32 major cities: spatial patterns and drivers. Remote Sens Environ 152:51–61. https://doi.org/10.1016/j.rse.2014.05.017